Radiation Physics and Chemistry xx (xxxx) xxxx–xxxx

Contents lists available at ScienceDirect

Radiation Physics and Chemistry

journal homepage: www.elsevier.com/locate/radphyschem

Compact energy dispersive X-ray microdiffractometer for diagnosis of neoplastic tissues

C. Sosa[a,b], A. Malezan[c], M.E. Poletti[c,*], R.D. Perez[a,b,**]

[a] Universidad Nacional de Córdoba, Ciudad Universitaria, Córdoba, Argentina
[b] Consejo Nacional de Investigaciones Científicas y Técnicas-CONICET, Buenos Aires, Argentina
[c] Departamento de Física da Faculdade de Filosofia, Ciências e Letras de Ribeirão Preto. Universidade de São Paulo, Brazil

ARTICLE INFO

Keywords:
Energy dispersive
X-ray microanalysis
XRD
Breast cancer

ABSTRACT

An energy dispersive X-ray microdiffractometer with capillary optics has been developed for characterizing breast cancer. The employment of low divergence capillary optics helps to reduce the setup size to a few centimeters, while providing a lateral spatial resolution of 100 μm. The system angular calibration and momentum transfer resolution were assessed by a detailed study of a polycrystalline reference material. The performance of the system was tested by means of the analysis of tissue-equivalent samples previously characterized by conventional X-ray diffraction. In addition, a simplified correction model for an appropriate comparison of the diffraction spectra was developed and validated. Finally, the system was employed to evaluate normal and neoplastic human breast samples, in order to determine their X-ray scatter signatures. The initial results indicate that the use of this compact energy dispersive X-ray microdiffractometer combined with a simplified correction procedure is able to provide additional information to breast cancer diagnosis.

1. Introduction

X-ray diffraction (XRD) and medical imaging techniques can be successfully combined to provide a powerful tool able to differentiate tissues with similar X-ray attenuation characteristics (Kosanetzky et al., 1987; Speller, 1999; Bradley and Wells, 2013; Harding and Schreiber, 1999). XRD analysis discriminates between glandular, adipose and neoplastic breast tissues becoming a helpful tool for breast cancer diagnosis (Speller, 1999; Kidane et al., 1999; Poletti et al., 2002a, 2002b; Cunha et al., 2006; Griffiths et al., 2007; Ryan and Farquharson, 2007; Oliveira et al., 2008; Pani et al., 2010). For this application, the Energy Dispersive X-Ray Diffraction (EDXRD) technique is useful to reduce the acquisition time and simplify the detection system (Clark, 2002). These advantages are consequence of employing a solid state detector with high energy resolution, which performs simultaneous energy scanning of the scattered beam, avoiding complex mechanical motions.

In an energy dispersive configuration, a polychromatic excitation beam with low divergence is required to apply the Bragg Law. Usually, it is obtained by means of the alignment of two small collimators with a large distance between them, in the order of several tens of centimeters (Kidane et al., 1999; Cunha et al., 2006; Ryan and Farquharson, 2007; Pani et al., 2010; LeClair et al., 2006; King and Johns, 2010; Chaparian et al., 2010; King et al., 2011; Abdelkader et al., 2012; Tang et al., 2014a, 2014b). In the present work, we showed that the employment of capillary optics in the excitation channel reduces this distance to a few centimeters, giving rise to a compact setup. In addition, the lens also reduces the excitation area, keeping a high photon flux over the sample, which allows X-ray microdiffraction analysis (micro-XRD).

2. EDXRD methodology

2.1. Basic principles

An energy dispersive micro-XRD (micro-EDXRD) system combines the EDXRD with the spatial resolution of the X-ray microanalysis. EDXRD is a well-known method, which can be implemented without complex mechanical detector or source motion, since the scattering angle is fixed. It takes advantage of the high energy resolution semiconductor X-ray detectors technology to electronically scan the scattered beam, looking for constructive interference peaks. In the case of crystals, these peaks originate from coherent scattering at different atomic planes, according to Bragg's condition:

** Corresponding author at: Universidad Nacional de Córdoba, Ciudad Universitaria, Córdoba, Argentina.
* Corresponding author at: Departamento de Física da Faculdade de Filosofia, Ciências e Letras de Ribeirão Preto. Universidade de São Paulo, Brazil.
E-mail addresses: poletti@ffclrp.usp.br (M.E. Poletti), danperez@famaf.unc.edu.ar (R.D. Perez).

http://dx.doi.org/10.1016/j.radphyschem.2016.11.005
Received 14 December 2015; Received in revised form 8 November 2016; Accepted 14 November 2016
Available online xxxx
0969-806X/

$$d = \frac{0.6199}{E \sin\theta} = \frac{1}{2x} \quad (1)$$

where d is the interplanar spacing of the lattice planes in nanometers (nm), 2θ is the scattering angle, E is energy of the scattered photon in keV and x is the momentum transfer, $x(nm^{-1}) = [E(keV)/1.2398]\sin(\theta)$. Thus, the energy of any particular diffraction peak depends upon the scattering angle. In particular, this angle is adjusted such that the diffraction peaks of interest fall in the useful range of X-ray flux available from the used source (Clark, 2002). The Full Width at Half Maximum (FWHM) of a diffraction peak (ΔE_{FWHM}) depends upon the angular resolution of the system ($\Delta\theta$) and the energy resolution of the detector (ΔE_D). For a single peak, the ΔE_{FWHM} can be taken as the minimum energy separation between two resolved diffraction peaks, i.e., as a measure of the system to resolve the peaks in the momentum transfer space (momentum transfer resolution, $\Delta x/x$).

The D-spacing resolution ($\Delta d/d = \Delta x/x$) can be estimated from $\Delta\theta$ and ΔE_D by means of statistical error propagation derived from the Eq. (1):

$$\left(\frac{\Delta d}{d}\right)^2 = (\Delta\theta ctg\theta)^2 + \left(\frac{\Delta E_D}{E}\right)^2 \quad (2)$$

Considering that a high energy resolution detector (HPGe, Si(Li) or SDD) is chosen for the system configuration, the improvement of the momentum transfer resolution mainly depends on the effectiveness of the strategies to reduce the angular divergence of the system, $\Delta\theta$. The latter is related to the divergences of incident and scattered beams. The employment of a focusing lens with low divergence reduces the incidence divergence. In addition, the small transversal section of the focalized incident beam combined with thin sample thickness allow a reduction of the target volume (range of scattered angles) keeping the sample-detector distance in the range of few centimeters.

2.2. The energy spectrum of the scattered X-ray photons

The energy distribution of the number of detected scattered photons, $N(E)$, has contributions from many background sources (air, sample holder and collimators) and includes single and multiple scattering within the sample. In this work, the multiple scattering is neglected, because sample dimensions were small compared to the mean free path of the scattered photons (Kidane et al., 1999). The background spectrum (all contributions), $N^B(E)$, was measured (in the absence of the sample, but remaining all other scatter conditions the same) and subtracted from the detected scattering X-ray spectra, weighting by the transmission factor of the sample (Geraldelli et al., 2013):

$$N^{corr}(E) = N(E) - N^B(E)e^{-\mu(E)t} \quad (3)$$

where $\mu(E)$ and t are the linear attenuation coefficient and thickness of the sample, respectively. Therefore, it is possible to assume that the corrected spectrum, $N^{corr}(E)$, is related solely to single scattering events at the sample and can be approximated as (Geraldelli et al., 2013):

$$N^{corr}(E) = \varepsilon(E)N_o(E)\eta\frac{d\sigma}{d\Omega}(E)\Omega_D G_T(E) \quad (4)$$

where $\varepsilon(E)$ is the detector efficiency at energy E, $N_o(E)$ is the number of photons incident on the sample, η is the number of atoms or molecules per unit of volume, $d\sigma/d\Omega(E)$ is the differential total scattering cross section of an atom or molecule, Ω_D is the solid angle subtended by the detector and $G_T(E)$ is an appropriate geometric transmission factor (which accounts for both sample self-attenuation and geometry). For the EDXRD setup, a fixed position for the X-ray detector was selected in order to define the scattering angle 2θ. Then, all the factors in the previous equation show variations only with the incident energy. In addition, the values adopted for 2θ are usually of a few degrees in order to neglect the energy variations produced by the incoherent scattering contribution (Clark, 2002). Thus, the differential total scattering cross section can be evaluated as $d\sigma/d\Omega(E) = [F^2(x) + F_{KN}.S(x)]d\sigma_{Th}/d\Omega$, where $d\sigma_{Th}/d\Omega$ is the Thomson differential cross section equal to $(r_o^2/2)(1 + \cos^2 2\theta)$, r_o is the classical electron radius, $F(x)$ is the atomic or molecular structural form factor, F_{KN} is the Klein-Nishina function and $S(x)$ in the incoherent scattering function. In the case of biological tissues, the form factor profile depends on intramolecular as well as intermolecular interference effects, giving rise to particular diffraction patterns for each tissue. On the other hand, the Compton contribution to the differential total scattering cross section is often ignored because it is small and structureless over the measured momentum transfer range (Geraldelli et al., 2013).

The geometric transmission factor, $G_T(E)$, can be calculated by:

$$G_T(E) = e^{-\mu(E)t/\cos 2\theta}\left[\frac{e^{[(1/\cos 2\theta)-1]\mu(E)t} - 1}{(1/\cos 2\theta - 1)\mu(E)}\right] \cong e^{-\mu(E)t/cos2\theta}t \quad (5)$$

The approximation equation is valid when the thickness is at least one order of magnitude smaller than the mean free path or for small angles such in our case.

3. Materials and methods

3.1. Instrumentation

The schematic diagram of the energy dispersive micro-XRD in transmission geometry employed in this work is shown in Fig. 1. The source was an W X-ray tube Philips model PW2275/20 operating at 60 kV–30 mA. The W anode was tilted 6° from the horizontal plane with focus dimension of 0.4 mm×12 mm, but it was oriented as to obtain a point source (0.4 mm×1.2 mm). Attached at the selected output, there was a high quality conical monocapillary made of borosilicate glass by drawing at high temperature in a heating furnace (Perez et al., 2008). Its inner diameter linearly decreases from 0.77 to 0.1 mm along 100 mm of length, providing an output divergence of 5 mrad. The lens was designed to produce a mean gain factor of 2 with a focal spot size of 100 μm at 3 mm of the tip. The wall of the lens was thick enough for an effective attenuation of the high energy X-ray photons. Radiation transport simulations were performed using a developed MATLAB® (MathWorks, USA) routine, which allows studying the energy dependence of transmission, divergence and focal size of the lens (Sosa et al., 2015).

The samples were placed 3 mm from the output of the lens. The diffraction angle 2θ was chosen as 7° in order to interrogate a momentum transfer region from 0.7 nm^{-1} to 2.5 nm^{-1}. This region corresponds to the range where most biological tissues exhibit interference effects (Speller, 1999; Kidane et al., 1999).

The scattered photons were collected by a SDD detector AMPTEK®. The distance from the entrance window of the detector and the surface sample was 70 mm. A 1 mm lead collimator delimited the acceptance angle of the detector. Acquisition time of 600 s was used to achieve appropriate statistical counting (i.e., uncertainties in the photon count smaller than 3% in the scattered energy spectra). The energy calibra-

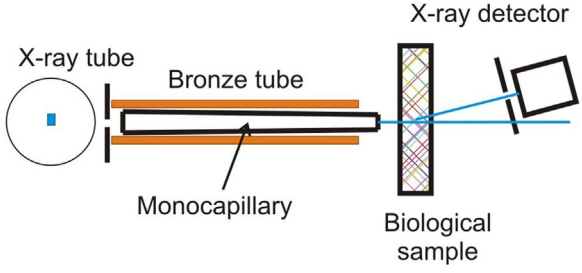

Fig. 1. Schematic diagram of the micro-EDXRD spectrometer presented in this work.

tion of the X-ray detector was carried out using calibration sources of ^{55}Fe and ^{241}Am.

3.2. Reference and tissue-equivalent materials

A reference powder quartz (SiO_2) sample was used to experimentally verify the actual scatter angle and determine the momentum transfer resolution of the micro-EDXRD system. The two highest intensity lines (011) and (100), with interplanar spacing of 3.34 Å and 4.25 Å respectively, were employed to perform this assessment. The measurement was repeated at least ten times to avoid mineral preferred orientation effects and spotty diffraction rings. The momentum transfer resolution obtained was 8%.

To test the methodology of collection and correction of experimental data, several tissue-equivalent samples: Polyacetate (CH_2O), Polyethylene (C_2H_4), Nylon ($C_6H_{11}NO$) and Teflon (C_2F_4) were measured and their scattering profiles were corrected and compared with those obtained by conventional X-ray diffraction. It is worthwhile to mention that these polymers show scattering profiles typical of amorphous materials similar to those from biological tissues (Kosanetzky et al., 1987; Poletti et al., 2002a, 2002b).

3.3. Breast tissue samples

A total of 60 human breast samples were analyzed with the diffractometer, 24 of them were classified as normal and the remaining were ductal carcinomas. All samples were obtained from patients submitted to surgical breast reduction mammoplasties and prophylactic mastectomies at Hospital das Clínicas from Faculdade de Medicina de Ribeirão Preto, Universidade de São Paulo in Ribeirão Preto, Brazil. Upon removal, the samples were fixed in formalin (4% formaldehyde in water) and stored at room temperature. Two adjacent pieces were cut from each specimen; the first one was stained with haematoxylin and eosin (H & $2E) and analyzed by two independent breast pathologists for tissue classification, while the second one was prepared to be used in micro-XRD experiments. The collection and handling of these samples were performed in compliance with the requirements established by the local ethics committee. Each sample was cut in cylindrical form with 4 mm diameter and 1 mm height (thickness). Before measuring, the formalin was withdrawn from the tissues and the thickness of each sample was measured with a precision dial gauge.

3.4. Data correction- a simplified model

The comparison of the scattering profiles of different samples requires a previous data correction procedure according to the following steps (based on Eq. (4)): normalization by (*i*) the incident spectrum (excitation spectrum); (*ii*) the detector efficiency; (*iii*) detection geometry and (*iv*) geometric transmission factor. If the excitation and detection conditions are unchanged, then a simplified correction procedure which only accounts for the attenuation of X-rays through the sample can be applied. It consists of evaluating the ratio between corrected spectrum, $N^{corr}(E)$, and the factor $G_T(E)$. For the evaluation of $G_T(E)$, the mass attenuation coefficient values of tissue-equivalent materials and breast samples were calculated using the mixture rule, considering the elemental composition given by Poletti et al. (2002a, 2002b) and the mass attenuation coefficient for each chemical element taken from XCOM database (Berger et al., 2005).

4. Results and discussions

Tissue-equivalent samples (Polyacetate, Polyethylene, Nylon and Teflon) were analyzed with the microdiffractometer and their corrected scattering profiles were compared with those obtained by conventional X-ray diffraction in Fig. 2. A qualitative comparison indicates that our microdiffractometer correctly discriminates the main structures (Harding and Schreiber, 1999; Griffiths et al., 2007) and shows a close agreement with the conventional XRD system. In addition, it shows that the compact setup provides enough momentum transfer resolution to identify the fine structural details contained in the scattering profiles of some tissue-equivalent materials as Polyethylene and Nylon (both materials have a partly crystalline structure). Also, in order to test the performance of the simplified correction model proposed in this work, pure Teflon samples with different thicknesses from 1 to 3 mm were analyzed. Fig. 3a and b show the raw and corrected diffraction patterns, respectively. Fig. 3a shows that the numbers of counts increased with the thickness of the sample (increasing the signal to noise ratio, SNR, e.g., for a sample of 3 mm the SNR is approximately 110% greater than that obtained with 1 mm). This fact can result in a practical advantage of reducing the counting times. Nevertheless, the increment of the thickness results in two types of deleterious effects on the diffraction patterns, a displacement and asymmetric broadening of diffraction peaks and an increasing of multiple scattering being detected. In addition, the use of thick samples has a negative effect on the momentum transfer resolution of the system (based on Eq. (2)). Fig. 3b shows that the agreement between the three patterns, after correction, is remarkably good. Fig. 3c illustrates the mean diffraction pattern (averaging for the three corrected patterns) together with the corresponding standard deviation as a function of the momentum transfer. As can be seen from the figure, the relative deviation of the corrected spectra was smaller than 10% over the diffraction peaks. Similar results were obtained for all other tissue-equivalent materials. Samples with a thickness larger than 1 mm were only analyzed to demonstrate the effectiveness of the correction procedure. These sample thicknesses have no practical use because they generate several deleterious effects as already cited.

Fig. 4 shows the mean scattering spectra for three types of human breast tissues corrected according to the proposed approach. Clear differences between adipose and others tissues are evidenced. Mean scattering profile of adipose tissue displays a sharp peak at 1.1 nm^{-1}, while the mean scattering profiles of normal glandular and ductal carcinoma show a broad peak at 1.5 nm^{-1}. The mean scattering profiles for normal glandular and ductal carcinoma breast tissues are quite similar, both showing a prominent peak at the same value of the momentum transfer. The only difference between them is the maximum intensity peak, which is smaller for the glandular profile. It agrees with previous reports obtained by conventional XRD (Ryan and Farquharson, 2007; Oliveira et al., 2008) or EDXRD (Kidane et al., 1999; Griffiths et al., 2007; LeClair et al., 2006). Within each tissue type, all corrected diffraction patterns were similar, with a mean relative standard deviation of 10%, 7% and 9% for adipose, glandular and ductal carcinomas groups, respectively. In order to identify the region of interest (or characteristic parameters as peak positions, intensities, full width half maximum, etc.) where these groups are statistically different, a multi comparison test was applied at each value of χ measured (or extracted parameter). Statistical results show that in all interval of χ measured (and all extracted parameters) adipose tissue is statistically different at the 5% significance level from all other investigated tissues, while the only functional parameter to differentiate glandular and ductal carcinoma was the peak intensity at the 15% significance level. Further research is still necessary in order to evaluate the precision of a diagnosis model based on the proposed approach.

In general, the obtained scattering profile shape and peak positions for each type of tissues and tissue-equivalent samples are in good agreement with those found in literature (Kidane et al., 1999; Poletti et al., 2002a, 2002b; Cunha et al., 2006; Griffiths et al., 2007; Ryan and Farquharson, 2007; Oliveira et al., 2008; Pani et al., 2010; LeClair et al., 2006; Geraldelli et al., 2013). Furthermore, it is remarkable that the proposed correction process avoids the excitation spectrum determination which is usually a cumbersome task. The corrected spectra combine the excitation spectrum profile with the scattering profile of the sample. Then, the comparison of the corrected spectra is valid only

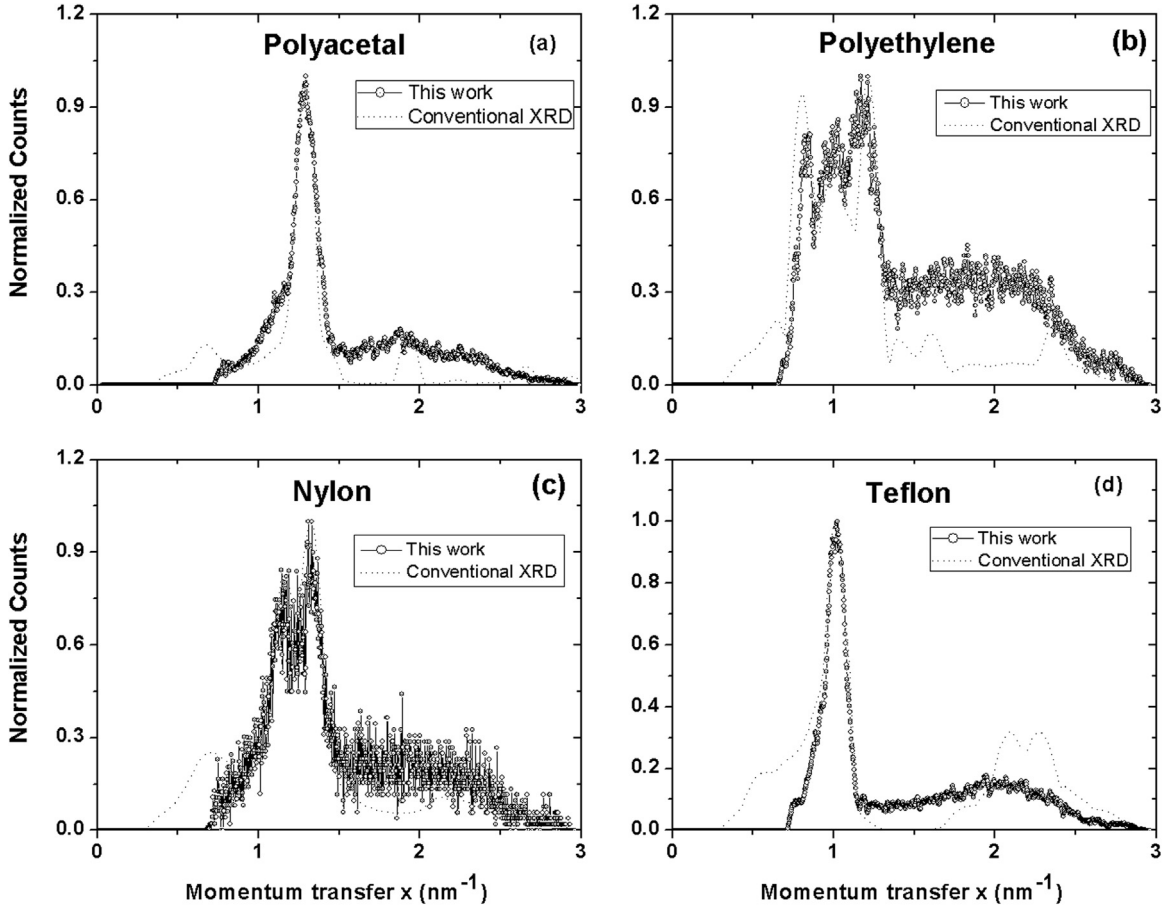

Fig. 2. Measured scattering profiles for four pure tissue-equivalent samples: (a) polyacetal, (b) polyethylene, (c) nylon and (d) teflon. The dot lines curves are the measurements for the same materials by conventional (angular dispersive) XRD.

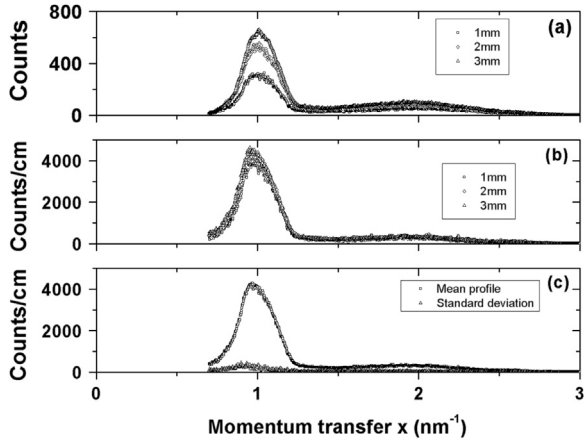

Fig. 3. a) Measured scattering profiles for three different thicknesses of Teflon foils: 1 mm (square dots), 2 mm (diamond dots) and 3 mm (triangle dots). b) The same profiles corrected by the transmission geometry factor (Eq. (4)). c) Mean corrected scattering profile for the three Teflon foils with the standard deviation.

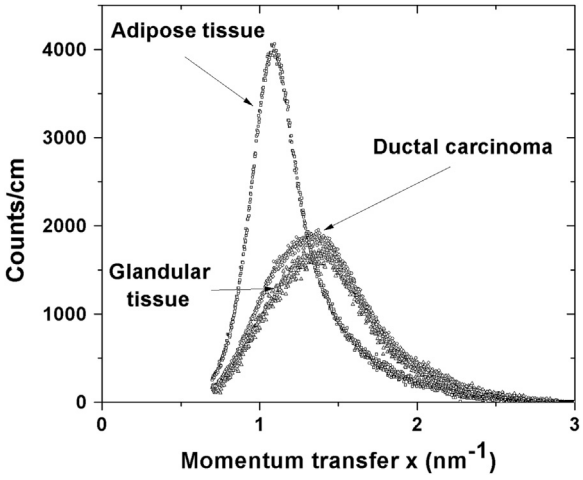

Fig. 4. Mean corrected scattering profiles for three types of human breast tissues. Significant differences between adipose, ductal carcinoma and normal glandular tissues were evidenced.

when they had been obtained under the same excitation conditions.

5. Conclusions

A successful compact energy dispersive X-ray micro-diffractometer with a lateral spatial resolution of 100 μm is presented in this work. The first results for the scattering profiles for some plastics and selected biological tissues were obtained. A simplified correction procedure to the raw-acquired spectra has been developed, allowing the identification of the main structural features on scattering profiles of amorphous samples. It is an encouraging result that motivates further studies to develop a diagnostic model of breast cancer based on these scattering profiles. In this sense, the spatial resolution of the micro-EDXRD helps to avoid the overlapping of scattering profiles due to the inhomogeneous nature of breast tissue, by means of a better definition of the irradiated area, thus showing potential for micro-EDXRD-based biopsy analysis of tissues.

Acknowledgments

Authors want acknowledgments to Eldereis de Paula and Carlos Renato da Silva for technical help. In addition, we also would like to thank the Department of Pathology of the Clinics Hospital, Faculty of Medicine of Ribeirão Preto, Brazil, for allowing collection of the human breast samples. Part of the work was carried within the framework of a Cooperation Research Project CAPES-MinCyT (Code BR1319 and 246/14). Finally, we thank the Brazilian agency Conselho Nacional de Desenvolvimento Científico e Tecnológico (CNPq) for partial financial support under grant number 460860/2014-3.

References

Abdelkader, M.H., Alkhateeb, S.M., Bradley, D.A., Pani, S., 2012. Development and characterization of a laboratory based X-ray diffraction imaging system for material and tissue characterization. Appl. Radiat. Isot. 70 (7), 1325–1330.

Berger M.J., Hubbell J.H., Seltzer, S.M., Chang, J., Coursey, J.S., Sukumar, R., Zucker, D. S., 2005. XCOM: Photon Cross Section Database (version 1.3). Avaliable at: ⟨http://physics.nist.gov/xcom⟩.

Bradley, D.A., Wells, K., 2013. Biomedical applications reviewed: hot topic areas. Rad. Phys. Chem. 85, 42–52.

Chaparian, A., Oghabian, M.A., Changizi, V., Farquharson, M.J., 2010. The optimization of an energy-dispersive X-ray diffraction system for potential clinical application. Appl. Radiat. Isot. 68 (12), 2237–2245.

Clark, S.M., 2002. Thirty years of energy-dispersive powder diffraction. Cryst. Rev. 8, 57–92.

Cunha, D.M., Oliveira, O.R., Pérez, C.A., Poletti, M.E., 2006. X-ray scattering profiles of some normal and malignant human breast tissues. X-Ray Spectrom. 35 (6), 370–374.

Geraldelli, W., Tomal, A., Poletti, M.E., 2013. Characterization of tissue-equivalent materials through measurements of the linear attenuation coefficient and scattering profiles obtained with polyenergetic beams. IEEE Trans. Nucl. Sci. 60 (2), 566–571.

Griffiths, J.A., Royle, G.J., Hanby, A.M., Horrocks, J.A., Bohndiek, S.E., Speller, R.D., 2007. Correlation of energy dispersive diffraction signatures and microCT of small breast tissue samples with pathological analysis. Phys. Med. Biol. 52 (20), 6151–6164.

Harding, G., Schreiber, B., 1999. Coherent X-ray scatter imaging and its applications in biomedical science and industry. Rad. Phys. Chem. 56, 229–245.

Kidane, G., Speller, R.D., Royle, G.J., Hanby, A.M., 1999. X-ray scatter signatures for normal and neoplastic breast tissues. Phys. Med. Biol. 44 (7), 1791–1802.

King, B.W., Johns, P.C., 2010. An energy-dispersive technique to measure x-ray coherent scattering form factors of amorphous materials. Phys. Med. Biol. 55 (3), 855–871.

King, B.W., Landheer, K.A., Johns, P.C., 2011. X-ray coherent scattering form factors of tissues, water and plastics using energy dispersion. Phys. Med. Biol. 56 (14), 4377–4397.

Kosanetzky, J., Knoerr, B., Harding, G., Neitzel, U., 1987. X-ray diffraction measurements of some plastic materials and body tissues. Med. Phys. 14, 526–532.

LeClair, R.J., Boileau, M.M., Wang, Y., 2006. A semianalytic model to extract differential linear scattering coefficients of breast tissue from energy dispersive x-ray diffraction measurements. Med. Phys. 33 (4), 959–967.

Oliveira, O.R., Conceição, A.L.C., Cunha, D.M., Poletti, M.E., Pelá, C.A., 2008. Identification of neoplasias of breast tissues using a powder diffractometer. J. Radiat. Res. 49 (5), 527–532.

Pani, S., Cook, E.J., Horrocks, J.A., Jones, J.L., Speller, R.D., 2010. Characterization of breast tissue using energy-dispersive X-ray diffraction computed tomography. Appl. Radiat. Isot. 68 (10), 1980–1987.

Perez, R.D., Sánchez, H.J., Rubio, M., Perez, C.A., 2008. Characterization of home-made X-ray polycapillaries. X-ray Spectrom. 37, 646–651.

Poletti, M.E., Gonçalves, O.D., Mazzaro, I., 2002a. Coherent and incoherent scattering of 17.44 and 6.93 keV x-ray photons scattered from biological and biological-equivalent samples: characterization of tissues. X-Ray Spectrom. 31 (1), 57–61.

Poletti, M.E., Gonçalves, O.D., Mazzaro, I., 2002b. X-ray scattering from human breast tissues and breast-equivalent materials. Phys. Med. Biol. 47, 47–63.

Ryan, E.A., Farquharson, M.J., 2007. Breast tissue classification using x-ray scattering measurements and multivariate data analysis. Phys. Med. Biol. 52 (22), 6679–6696.

Sosa, C., Stoytschew, V., Leani, J., Sánchez, H.J., Perez, C., Perez, R.D., 2015. Calibration method for confocal x-ray microanalysis withpolychromatic excitation. J. Spectrosc. 2015, 1–7.

Speller, R., 1999. Tissue analysis using x-ray scattering. X-Ray Spectrom. 28, 244–250.

Tang, R.Y., Laamanen, C., McDonald, N., Leclair, R.J., 2014a. WAXS fat subtraction model to estimate differential linear scattering coefficients of fatless breast tissue: phantom materials evaluation. Med. Phys. 41 (5), 53501.

Tang, R.Y., McDonald, N., Laamanen, C., Leclair, R.J., 2014b. A method to estimate the fractional fat volume within a ROI of a breast biopsy for WAXS applications: animal tissue evaluation. Med. Phys. 41 (11), 113501.